Double sinusoidal phase-modulating distributed-Bragg-reflector laser-diode interferometer for distance measurement

Takamasa Suzuki, Hiromi Suda, and Osami Sasaki

A previously proposed double sinusoidal phase-modulating (DSPM) laser-diode interferometer measures distances larger than a half-wavelength by detecting modulation depth. Although it requires a vibrating mirror to provide the second modulation to the interference signal, such vibrations naturally affect measurement accuracy. We propose a static-type DSPM laser-diode interferometer that uses no mechanical modulation. Our experimental results indicate a measurement error of ± 1.6 μm. © 2003 Optical Society of America

OCIS codes: 120.3180, 150.5670, 120.3940, 120.5050, 120.5060, 140.2020.

1. Introduction

In standard laser interferometers, since the optical path distance (OPD) is detected from a phase change of between 0 and 2π, an OPD greater than the optical wavelength cannot be measured. To overcome this problem, interferometries that use two or more wavelengths have been proposed.[1,2] Because two-wavelength interferometers use two separate laser sources, it is difficult to align the optical axes and the setup is complicated. When laser diodes (LDs) are used,[3] the setup is more compact. Optical alignment, on the other hand, is complicated. A single LD has been used in absolute distance measurements.[4,5] Although the optical setup in these devices is simple, measurement accuracy is ~20 μm. So a more precise measurement system has been a long-term goal. We have proposed a double sinusoidal phase-modulating (DSPM) interferometer capable of measuring distances greater than a half-wavelength with a single LD.[6] With this device the interference signal detected by the Twyman–Green interferometer contains two different sinusoidal phase modulations produced by carrier and modulating signals.

The authors are with Faculty of Engineering, Niigata University, 8050 Ikarashi 2, Niigata, 950-2181 Japan (e-mail for T. Suzuki, takamasa@eng.niigata-u.ac.jp).

Received 6 May 2002; revised manuscript received 26 August 2002.

0003-6935/03/010060-07$15.00/0

The amplitude of the phase modulation, which is proportional to the OPD, is used to detect the distance. Although in the DSPM interferometer previously proposed the carrier signal was applied mechanically by a vibrating mirror driven by a piezoelectric transducer (PZT), it is far more desirable that the interferometer be static. A PZT especially has a few kilohertz of low-frequency response and nonlinearity. Moreover, even if the system is modified to a two-dimensional system that measures a large testing area, we need not move the heavy reference mirror in the static measurement system. The static operation prevents the reference mirror from deformation caused by mechanical movement. That is, we want to avoid the use of mechanical phase modulators.

The LD is suitable from this point of view because it can easily be tuned by the injection current. Current modulation, however, changes not only the wavelength but also the optical power of the laser beam. Therefore the interference signal includes useless intensity modulation. In an actual measurement this intensity modulation results in measurement error. Especially in the DSPM interferometer the intensity modulation created by the carrier signal induces a measurement error, while the intensity modulation created by the modulating signal does not affect measurement accuracy. Moreover the detection sensitivity for the phase-modulation amplitude is low because of the narrow tuning range of the wavelength.

In this paper we apply a distributed-Bragg-reflector (DBR) LD to the DSPM interferometer, dem-

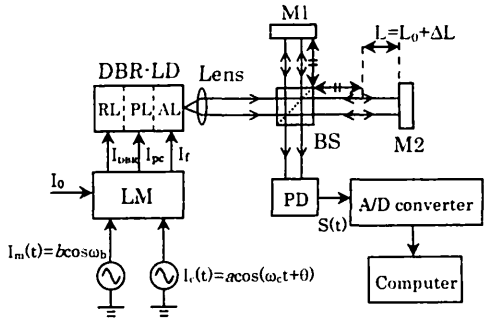

Fig. 1. Experimental setup: M1, M2, mirrors; BS, beam splitter; PD, photodiode; LM, laser-diode modulator; RL, reflection-tuning layer; PL, phase-tuning layer; AL, active layer.

onstrating distance measurement. The DBR LD provides a wide range of wavelength tuning with a low-intensity modulation. This wide tuning range enables us to detect distance accurately. The prototype system described in this paper requires no mechanical vibration for the phase modulation. So we can construct a static interferometer, which indicates a measurement error as small as ± 1.6 μm.

2. Principle

A. Double Sinusoidal Phase Modulation

Figure 1 shows a DSPM interferometer with a DBR LD for distance measurement. The OPD of the Twyman–Green interferometer is $2L$. The injection current of the LD modulator, LM, consists of sinusoidal currents

$$I_c(t) = a \cos(\omega_c t + \theta), \tag{1}$$

$$I_m(t) = b \cos \omega_b t, \tag{2}$$

and a dc bias current I_0, where $\omega_b \ll \omega_c$ and $a \ll b$.

For clarification we refer to $I_c(t)$ and $I_m(t)$ as the carrier and modulating signals, respectively. Modulation by these injection currents results in both the wavelength modulation

$$\lambda(t) = \lambda_0 + \Delta\lambda_a \cos(\omega_c t + \theta) + \Delta\lambda_b \cos \omega_b t \tag{3}$$

and the intensity modulation

$$g(t) = g_0[1 + \gamma a \cos(\omega_c t + \theta) + \gamma b \cos \omega_b t], \tag{4}$$

where $\Delta\lambda_a = \beta a$ and $\Delta\lambda_b = \beta b$ are amplitudes of the wavelength shift, λ_0 is the central wavelength, and g_0 is the average intensity; β represents the ratio between the wavelength change and the injection current and is referred to as modulation efficiency; γ is a coefficient of the optical power change stimulated by the injection current.

The interference signal detected with a photodiode, PD, is given by

$$S(t) = g(t)\{1 + V \cos[Z_c \cos(\omega_c t + \theta) - \Phi(t)]\}. \tag{5}$$

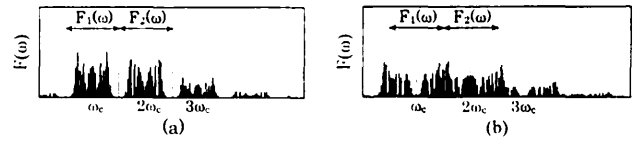

Fig. 2. Frequency components embraced in $S(t)$. $F_1(\omega)$ and $F_2(\omega)$ are (a) separated and (b) not separated on the frequency plane.

where the modulation amplitude Z_c and the desired phase $\Phi(t)$ are expressed by

$$Z_c = 4\pi\Delta\lambda_a L/\lambda_0^2, \tag{6}$$

$$\Phi(t) = Z_b \cos \omega_b t + \alpha, \tag{7}$$

respectively, and V represents visibility. Amplitude Z_b and phase α in $\Phi(t)$ are given as

$$Z_b = 4\pi\Delta\lambda_b L/\lambda_0^2, \tag{8}$$

$$\alpha = 4\pi L/\lambda_0, \tag{9}$$

respectively. Thus the distance L is given by

$$L = \frac{\lambda_0^2}{4\pi\Delta\lambda_b} Z_b. \tag{10}$$

In DSPM interferometry we use a large modulation-current amplitude so as to introduce a large wavelength shift $\Delta\lambda_b$. The large intensity modulation $g(t)$, however, accompanies the interference signal.

B. Signal Processing

Although DSPM signal processing was shown in Ref. 6, we explain it here in greater detail. $S(t)$ in Eq. (5) is expanded to

$$\begin{aligned} S(t) = g(t) &+ \{g(t)V \cos \Phi(t)\}[J_0(Z_c) \\ &- 2J_2(Z_c)\cos(2\omega_c t + 2\theta) + \cdots] \\ &- \{g(t)V \sin \Phi(t)\}[2J_1(Z_c)\cos(\omega_c t + \theta) \\ &- 2J_3(Z_c)\cos(3\omega_c t + 3\theta) + \cdots] \end{aligned} \tag{11}$$

through the use of frequency components, where $J_n(Z)$ is the nth-order Bessel function. The lower-frequency components in braces in Eq. (11) are illustrated in Fig. 2. The Fourier transform of $S(t)$ is given by

$$\begin{aligned} F(\omega) = \Im[g(t)] &+ \Im[g(t)V \cos\{\Phi(t)\}] \\ &* \left[\sum_{m=-\infty}^{\infty} (-1)^m J_{2m}(Z_c)\exp(j2m\theta)\delta(\omega \right. \\ &\left. - 2m\omega_c)\right] + \Im[g(t)V \sin\{\Phi(t)\}] \\ &* \left\{\sum_{m=-\infty}^{\infty} (-1)^m J_{2m-1}(Z_c)\exp[j(2m-1)\theta]\right. \\ &\left. \times \delta[\omega - (2m-1)\omega_c]\right\}, \end{aligned} \tag{12}$$

where $\Im[\ ]$ is the Fourier transformation of the argument and $*$ is a convolution. We denote the frequency components that lie in the region of $\omega_c/2 < \omega \le 3\omega_c/2$ and $3\omega_c/2 < \omega \le 5\omega_c/2$ as $F_1(\omega)$ and $F_2(\omega)$, respectively. If conditions

$$\Im[g(t)V \sin \Phi(t)] = 0 \quad |\omega| > \omega_c/2, \tag{13}$$

$$\Im[g(t)V \cos \Phi(t)] = 0 \quad |\omega| > \omega_c/2 \tag{14}$$

are satisfied, $F_1(\omega)$ and $F_2(\omega)$ are separated on the frequency plane as shown in Fig. 2(a). In this case, when $F_1(\omega)$ and $F_2(\omega)$ are shifted by ω_c and $2\omega_c$, respectively, toward the point of origin, the carrier components introduced by $I_c(t)$ are eliminated. We then arrive at

$$F_1(\omega + \omega_c) = -J_1(Z_c)\exp(j\theta)\Im[g(t)V \sin \Phi(t)], \tag{15}$$

$$F_2(\omega + 2\omega_c) = -J_2(Z_c)\exp(j2\theta)\Im[g(t)V \cos \Phi(t)]. \tag{16}$$

To determine the coefficients $J_n(Z_c)$ and $\exp(jn\theta)$ $(n = 1, 2)$, we set modulating signal $I_m(t)$ to zero and measure amplitude Z_c and argument θ experimentally with sinusoidal phase-modulating interferometry.[7] Amplitude Z_c especially is determined by the ratio $R = |J_3(Z_c)/J_1(Z_c)|$. $\Phi(t)$ is then calculated by

$$\Phi(t) = \tan^{-1}\left[\frac{g(t)V \sin \Phi(t)}{g(t)V \cos \Phi(t)}\right] = \tan^{-1}\left\{\frac{\Im^{-1}[\{F_1(\omega + \omega_c)\}/J_1(Z_c)\exp(j\theta)]}{\Im^{-1}[\{F_2(\omega + 2\omega_c)\}/J_2(Z_c)\exp(j2\theta)]}\right\}, \tag{17}$$

where $\Im^{-1}[\ ]$ gives an inverse Fourier transform of the argument. In this signal processing, intensity modulation $g(t)$ is perfectly canceled by the division operation in Eq. (17). Amplitude Z_b, which is the amplitude of frequency component ω_b, is easily obtained with the Fourier transform of $\Phi(t)$. We are then able to measure distance L with the formula shown in Eq. (10).

3. Error Analysis

A. Intensity Modulation

We show that the intensity modulation $g(t)$ is totally canceled in DSPM interferometry. The change in intensity that corresponds to the carrier signal $I_c(t)$, however, gives slight errors in detection of Z_c. We investigated these errors by using simulations, the parameters of which were $Z_b = 20$ rad, $Z_c = 2.5$ rad, $\theta = 0.5$ rad, $\alpha = 1.5$ rad, $\omega_b/2\pi = 100$ Hz, and $\omega_c/2\pi = 6.4$ kHz.

First, we calculated Z_c and Z_b with respect to γb in conditions of $\gamma a = 0$ to confirm the elimination of intensity modulation in DSPM interferometry; γb was varied from 0 to 0.5 at intervals of 0.1. In these calculations, no errors were detected on Z_c and Z_b as shown in Figs. 3(a) and 3(b), respectively. It indicates that DSPM interferometry effectively eliminates the intensity modulation related to the modulating signal. The change in Z_c and Z_b with respect to γa are calculated in conditions of $\gamma b = 0$. Results are shown in Fig. 4. The γa was also varied from 0 to 0.5 at an interval of 0.1. We can find that the errors in Z_b and Z_c become larger as γa increases. Therefore, to ensure overall measurement accuracy, γa is kept as small as possible. In such cases the DBR LDs are useful for reducing changes in intensity.

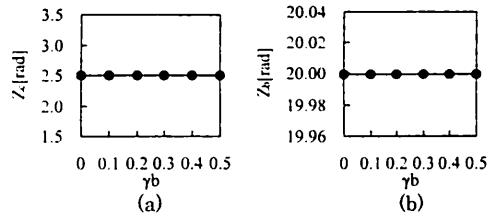

Fig. 3. Calculations of (a) Z_c and (b) Z_b with respect to γb in the conditions of $\gamma a = 0$.

B. Overlap of the Spectra

The DSPM interferometer previously proposed[6] used a PZT to provide phase modulation $a \cos(\omega_c t + \theta)$. Thus the phase modulation can be achieved even if the OPD is small. Then Z_b is also small enough to satisfy the conditions shown in Eqs. (13) and (14). On the other hand, our system requires several millimeters of OPD, because no phase modulation is achieved in the current modulation when the OPD is zero as shown in Eqs. (6) and (8). When Z_b becomes greater in accordance with the increase in injection current, the harmonics of ω_b around the carrier component $n\omega_c$ spread, and some harmonics overlap others around the next carrier component $(n + 1)\omega_c$ as shown in Fig. 2(b). In this case a separation between $F_1(\omega)$ and $F_2(\omega)$ is impossible and the value of Z_b cannot be calculated correctly. Therefore we investigated the maximum Z_b, which produces no spectral overlap between $F_1(\omega)$ and $F_2(\omega)$, by using a simulation. The calculations were performed with ratios between ω_c and ω_b of 32, 64, and 128. Results are shown in Fig. 5. The given and the calculated values of Z_b are shown on the horizontal and vertical axes, respectively. Figure 5 shows that we have to set large ratios between ω_c and ω_b to detect Z_b accurately.

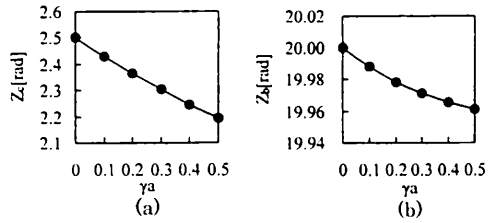

Fig. 4. Calculations of (a) Z_c and (b) Z_b with respect to γa in the conditions of $\gamma b = 0$.

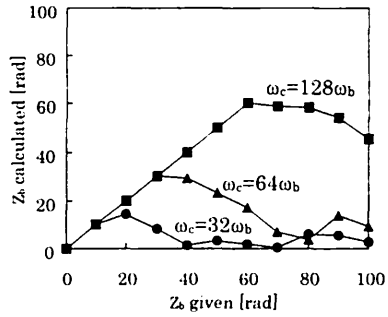

Fig. 5. Calculations of Z_b in the conditions of $\omega_c = 32\omega_b$, $\omega_c = 64\omega_b$, and $\omega_c = 128\omega_b$.

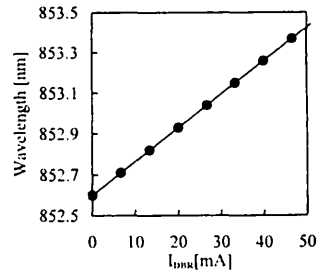

Fig. 6. DBR LD wavelength change according to I_{DBR}. The ratio between I_{pc} and I_{DBR} is 1:1.4.

C. Measurement Resolution, Error, and Range

Differentiating Eq. (11), we can derive

$$\delta L = \frac{\lambda_0^2}{4\pi\Delta\lambda_b}\delta Z_b. \tag{18}$$

Equation (18) indicates that the resolution depends on the wavelength shift $\Delta\lambda_b$ and Z_b terms detecting resolution. If the resolution of the Z_b terms is the same as that of the previously proposed DSPM interferometer, the resolution in the distance measurement is much improved when $\Delta\lambda_b$ is increased. δZ_b is determined by the temporal fluctuation in actual measurement.

Moreover, even if Z_b contains an error ε_Z in signal processing, the error appears as $\varepsilon_L = K\varepsilon_Z/\Delta\lambda_b$ in the distance measurement, where $K = \lambda_0^2/4\pi$ is a constant. Thus the error in signal processing is reduced when $\Delta\lambda_b$ increases from use of the DBR LD.

The measurement range is determined by $Z_{b\,\max}$ and $Z_{c\,\min}$, which are the maximum Z_b and the minimum Z_c, respectively. The maximum distance obviously depends on $Z_{b\,\max}$. Figure 5 shows that $Z_{b\,\max} = 30$ at $\omega_c = 64\omega_b$, which is used in the experiments as discussed below. On the other hand, the minimum distance does not depend on wide-wavelength tunability but on $Z_{c\,\min}$. Because we have to use a small carrier signal to avoid the intensity modulation in the detection of Z_c as described in Subsection 3.A, the wavelength shift $\Delta\lambda_a$ is not as large in Z_c. The signal processing in the DSPM interferometry is based on the sinusoidal phase-modulating interferometry that has been proposed in Ref. 7. We determined $Z_{c\,\min} = 1.4$ from the theoretical calculation of $R = |J_3(Z_c)/J_1(Z_c)| = 0.1$, which is the lowest ratio for determining Z_c in the previous experiments.[7] Therefore the measurement range is given by

$$\frac{\lambda_0^2}{4\pi\Delta\lambda_a} Z_{c\,\min} \le L \le \frac{\lambda_0^2}{4\pi\Delta\lambda_b} Z_{b\,\max}. \tag{19}$$

4. Experiments

A. Setup

The experimental setup is shown in Fig. 1. The wavelength and maximum output power of the DBR LD (Yokogawa Model YL85XTW) are 852 nm and 10 mW, respectively. The sinusoidal carrier signal $I_c(t)$ and modulating signal $I_m(t)$ (whose frequencies are 6.4 kHz and 100 Hz, respectively) are injected into the LD. The beam radiating from the LD is fed into a Twyman–Green interferometer whose initial OPD $2L_0$ is ~4 mm. The distance change is represented by ΔL.

The interference signal $S(t)$ detected by the PD is sampled with an analog-to-digital converter. The sampling frequency and number were 16 times the carrier frequency $\omega_c/2\pi$ and 4096, respectively.

B. Features of the DBR LD

The DBR LD possesses three electrodes that inject the forward current I_f, the phase-tuning current I_{pc}, and the reflection-tuning current I_{DBR} (Ref. 8) as shown in Fig. 1. The optical power mainly depends on I_f, which is injected into the active layer, AL. I_{pc} and I_{DBR} change not only the refractive indices but also the amount of light absorptions of both the phase-tuning layer, PL, and the reflection-tuning layer, RL, respectively. Although variation of the refractive indices changes the wavelength, the absorption affects the optical power to some degree. Usually optical power decreases according to the increments of I_{pc} and I_{DBR}. However, variation of the optical power is much smaller than that of conventional LDs. The ratio between I_{pc} and I_{DBR} must be maintained at 1:1.4–1.5 to prevent mode-hopping. We measured the wavelength by changing I_{DBR} where the ratio between I_{pc} and I_{DBR} was 1:1.4. The result is shown in Fig. 6. The wavelength changed by ~0.8 nm without mode-hopping. The modulation efficiency β is estimated to be 1.65×10^{-2} nm/mA as an inclination of the result. This value is ~4 times that of a multi-quantum-well LD. Since we can inject a large modulating current, the wavelength can be varied by as much as 1.6 nm under the absolute maximum rating provided by Yokogawa.

We measured the DBR LD's frequency response in a wavelength modulation. The frequency-based variation in modulation efficiency β is illustrated in Fig. 7. The cutoff frequency of β is estimated to be 6 kHz.

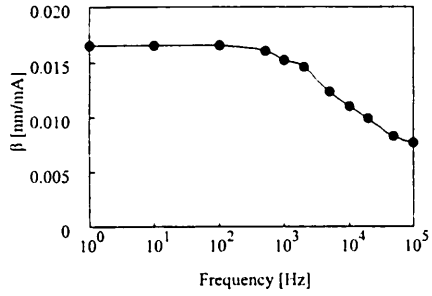

Fig. 7. Frequency response of the modulation efficiency β.

C. Observation of Interference Signals and Intensity Changes

We observed modulated interference signals and their coincidental intensity changes. Interference signals modulated by $I_c(t)$ and $I_m(t)$ are shown in Figs. 8(a) and 8(b), respectively. The modulation amplitude and the frequency of $I_c(t)$ and $I_m(t)$ are a = 3.5 mA, $\omega_c/2\pi$ = 6.4 kHz and b = 22.5 mA, $\omega_b/2\pi$ = 100 Hz, respectively. These parameters are used in the following experiments. The ratio between ω_c and ω_b is 64. Figure 8 confirms that the wavelength is modulated without mode-hopping. Amplitudes of the wavelength shift are estimated as $\Delta\lambda_a = \beta a = 5.8 \times 10^{-3}$ nm and $\Delta\lambda_b = \beta b = 0.37$ nm. The measurement range is then estimated from Eq. (19) as 1.40 mm $\leq L \leq$ 4.68 mm in conditions of $Z_{c\,\min} = 1.4$ rad and $Z_{b\,\max} = 30$ rad.

The intensity changes induced by $I_c(t)$ and $I_m(t)$ are shown in Figs. 9(a) and 9(b), respectively. The parameters of $I_c(t)$ and $I_m(t)$ are the same as those used in Fig. 8. The intensity change γa observed in Fig. 9(a) is 2.30×10^{-2} mW. Therefore the coefficient γ is calculated as 6.57×10^{-3} mW/mA. It results in an error in Z_b of 0.5×10^{-3} rad, which is calculated by the simulation shown in Fig. 4(b). The intensity change caused by $I_m(t)$ is large, as shown in Fig. 9(b),

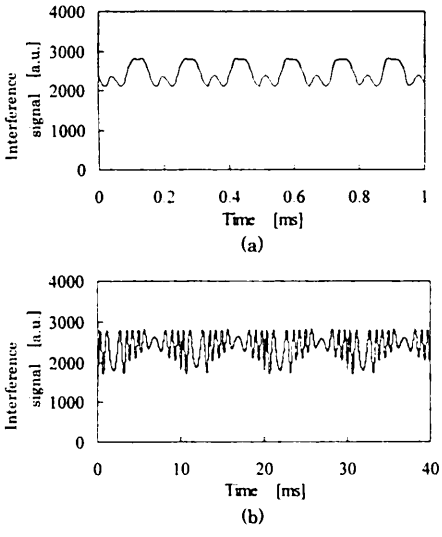

Fig. 8. Observed interference signals modulated by (a) $I_c(t)$ and (b) $I_m(t)$.

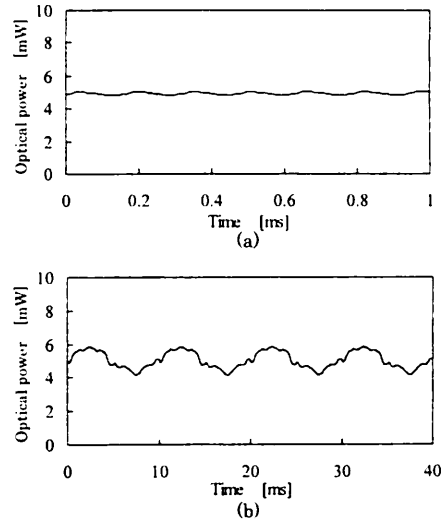

Fig. 9. Observed intensity changes induced by (a) $I_c(t)$ and (b) $I_m(t)$.

because of the light absorption described in Subsection 4.B. This change, however, is completely eliminated by the division operation as explained above.

D. Signal-Processing Observations

A typical instance of signal processing is shown in Fig. 10. The interference signal $S(t)$ modulated with both $I_c(t)$ and $I_m(t)$ is shown in Fig. 10(a). Results of the Fourier transform of $S(t)$ is shown in Fig. 10(b). The harmonics of ω_b are distributed around the carrier components $n\omega_c$, satisfying the conditions shown in Eqs. (13) and (14). The phase $\Phi(t)$ calculated from the frequency components, $F_1(\omega)$ and $F_2(\omega)$, is shown in Fig. 10(c). The frequency of $\Phi(t)$ shown in Fig. 10(c) agrees with the modulating frequency $\omega_b/2\pi$ = 100 Hz. Amplitude Z_b of $\Phi(t)$ calculated by the Fourier transform is shown in Fig. 10(d).

E. Distance Measurement

We moved M2 at intervals of ΔL = 0.1 mm. At each position we measured the value of Z_b. Results are shown in Fig. 11. The relationship between ΔL and Z_b is shown in Fig. 11. The initial value of Z_b was 13.849 rad at ΔL = 0 mm. It corresponds to an initial distance L_0 of 2.164 mm. Z_b (rad) = $6.4 \times 10^3 \times$ L (m) is obtained from the gradient of the line shown in Fig. 11. The coefficient 6.4×10^3 rad/m corresponds with the theoretical calculation from Eq. (8) in which λ_0 = 852 nm and $\Delta\lambda_b$ = 0.37 nm are used. The actual distance in each measurement is given in Fig. 12. The measurement starts at the initial distance L_0 of 2.164 mm.

Next we measured Z_b 10 times at the same OPD at intervals of a few minutes to estimate the temporal fluctuation of Z_b. Three kinds of distance were used in these experiments, the results of which are in Fig. 13. The fluctuation of Z_b was $\pm 1.0 \times 10^{-2}$ rad in rms. The measurement error is determined according to this fluctuation and is estimated at ± 1.6 μm.

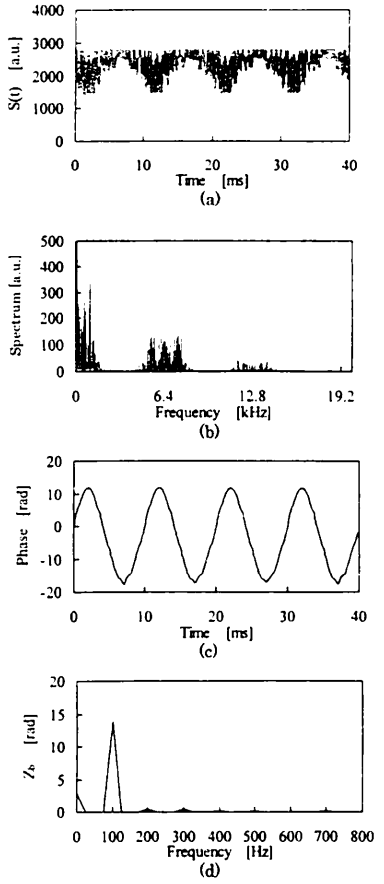

Fig. 10. Schematic of the signal processing: (a) DSPM interference signal $S(t)$, (b) result of the Fourier transform of $S(t)$, (c) phase $\Phi(t)$ calculated from $F_1(\omega)$ and $F_2(\omega)$, and (d) amplitude Z_b of $\Phi(t)$ calculated by the Fourier transform.

Vast improvement in measurement accuracy is expected through use of a feedback control system.[9] In DSPM interferometry we have to devise a generation of the feedback signal. We sample and hold $S(t)$ at the specific time when $I_c(t)$ crosses zero. Then we have interference signal $S_h(t)$ that is equivalently modulated only by $I_m(t)$. Multiplying $S_h(t)$ with $I_m(t)$ and passing it to a low-pass filter, we have the feedback signal.[9] When this feedback signal is added to $I_m(t)$ and fed into the DBR LD through an amplifier, we can eliminate external disturbance.

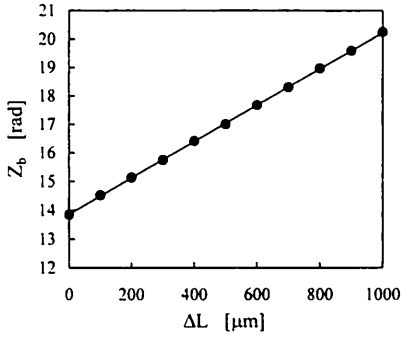

Fig. 11. Relationship between ΔL and Z_b.

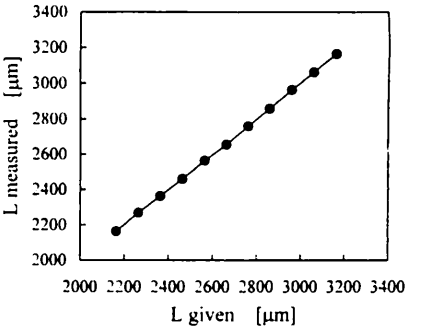

Fig. 12. Distances measured at intervals of ΔL = 0.1 mm.

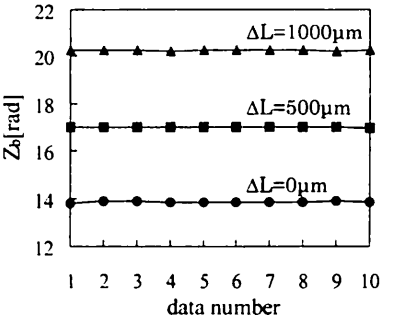

Fig. 13. Temporal fluctuations of Z_b at three kinds of OPD.

Although the feedback control was implemented mechanically by using the PZT in Ref. 6, the system proposed in this paper is able to realize feedback control with no mechanical devices.

5. Conclusion

A distributed-Bragg-reflector laser diode has been applied to the DSPM interferometer for distance measurement. It required no mechanical movement to provide the phase modulations. Therefore we could construct a static-type DSPM interferometer. The error caused by a change in the intensity of the optical power has been examined with a theoretical calculation. The experimental results have also indicated that our prototype system is immune to changes in measurement intensity. Measurement resolution, error, and range have been discussed. The wide wavelength tunability of the DBR LD enabled us to improve measurement resolution and error. The accuracy has been estimated from several measurements to be ± 1.6 μm.

References

1. Y.-Y. Cheng and J. C. Wyant, "Two-wavelength phase shifting interferometry," Appl. Opt. **23**, 4539–4543 (1984).
2. Y.-Y. Cheng and J. C. Wyant, "Multiple-wavelength phase-shifting interferometry," Appl. Opt. **24**, 804–807 (1985).
3. A. J. den Boef, "Two-wavelength scanning spot interferometer using single-frequency diode lasers," Appl. Opt. **27**, 306–311 (1988).
4. C. C. Williams and H. K. Wickramasinghe, "Optical ranging by

wavelength multiplexed interferometry," J. Appl. Phys. **60,** 1900–1903 (1986).
5. T. Suzuki, O. Sasaki, and T. Maruyama, "Absolute distance measurement using wavelength-multiplexed phase-locked laser diode interferometry," Opt. Eng. **35,** 492–497 (1996).
6. O. Sasaki, T. Yoshida, and T. Suzuki, "Double sinusoidal phase-modulating laser diode interferometer for distance measurement," Appl. Opt. **30,** 3617–3621 (1991).
7. O. Sasaki and H. Okazaki, "Sinusoidal phase-modulating interferometry for surface profile measurement," Appl. Opt. **25,** 3137–3140 (1986).
8. G. Mourat, N. Servagent, and T. Bosch, "Distance measurement using the self-mixing effect in a three electrode distributed Bragg reflector laser diode," Opt. Eng. **39,** 738–743 (2000).
9. O. Sasaki, K. Takahashi, and T. Suzuki, "Sinusoidal phase-modulating laser diode interferometer with a feedback control system to eliminate external disturbance," Opt. Eng. **29,** 1511–1515 (1990).